

12-23-2019

High-voltage vertical Ga₂O₃ power rectifiers operational at high temperatures up to 600 K

Boyan Wang
Virginia Polytechnic Institute and State University

Ming Xiao
Virginia Polytechnic Institute and State University

Xiaodong Yan
University of Southern California

Hiu Yung Wong
San Jose State University, hiuyung.wong@sjsu.edu

Jiahui Ma
University of Southern California

See next page for additional authors

Follow this and additional works at: https://scholarworks.sjsu.edu/faculty_rsca

Recommended Citation

Boyan Wang, Ming Xiao, Xiaodong Yan, Hiu Yung Wong, Jiahui Ma, Kohei Sasaki, Han Wang, and Yuhao Zhang. "High-voltage vertical Ga₂O₃ power rectifiers operational at high temperatures up to 600 K" *Applied Physics Letters* (2019). <https://doi.org/10.1063/1.5132818>

This Article is brought to you for free and open access by SJSU ScholarWorks. It has been accepted for inclusion in Faculty Research, Scholarly, and Creative Activity by an authorized administrator of SJSU ScholarWorks. For more information, please contact scholarworks@sjsu.edu.

Authors

Boyan Wang, Ming Xiao, Xiaodong Yan, Hiu Yung Wong, Jiahui Ma, Kohei Sasaki, Han Wang, and Yuhao Zhang

High-voltage vertical Ga₂O₃ power rectifiers operational at high temperatures up to 600 K

EP

Cite as: Appl. Phys. Lett. **115**, 263503 (2019); <https://doi.org/10.1063/1.5132818>

Submitted: 20 October 2019 • Accepted: 16 December 2019 • Published Online: 27 December 2019

Boyan Wang, Ming Xiao,  Xiaodong Yan, et al.

COLLECTIONS

EP

This paper was selected as an Editor's Pick



View Online



Export Citation



CrossMark

ARTICLES YOU MAY BE INTERESTED IN

[A review of Ga₂O₃ materials, processing, and devices](#)

Applied Physics Reviews **5**, 011301 (2018); <https://doi.org/10.1063/1.5006941>

[1-kV vertical Ga₂O₃ field-plated Schottky barrier diodes](#)

Applied Physics Letters **110**, 103506 (2017); <https://doi.org/10.1063/1.4977857>

[Gallium oxide \(Ga₂O₃\) metal-semiconductor field-effect transistors on single-crystal β-Ga₂O₃ \(010\) substrates](#)

Applied Physics Letters **100**, 013504 (2012); <https://doi.org/10.1063/1.3674287>



Time to get excited.
Lock-in Amplifiers – from DC to 8.5 GHz

[Find out more](#)

 Zurich Instruments

High-voltage vertical Ga₂O₃ power rectifiers operational at high temperatures up to 600 K EP

Cite as: Appl. Phys. Lett. **115**, 263503 (2019); doi: [10.1063/1.5132818](https://doi.org/10.1063/1.5132818)

Submitted: 20 October 2019 · Accepted: 16 December 2019 ·

Published Online: 27 December 2019






View Online



Export Citation



CrossMark

Boyan Wang,¹ Ming Xiao,¹ Xiaodong Yan,²  Hiu Yung Wong,³  Jiahui Ma,² Kohei Sasaki,⁴ Han Wang,^{2,a)} and Yuhao Zhang^{1,a)} 

AFFILIATIONS

¹Center for Power Electronics Systems, The Bradley Department of Electrical and Computer Engineering, Virginia Polytechnic Institute and State University, Blacksburg, Virginia 24061, USA

²Ming Hsieh Department of Electrical Engineering, University of Southern California, Los Angeles, California 90086, USA

³The Electrical Engineering Department, San Jose State University, San Jose, California 95192, USA

⁴Novel Crystal Technology, Inc., Sayama 350-1328, Japan

^{a)}Authors to whom correspondence should be addressed: han.wang.4@usc.edu and yhzhang@vt.edu

ABSTRACT

This work presents the temperature-dependent forward conduction and reverse blocking characteristics of a high-voltage vertical Ga₂O₃ power rectifier from 300 K to 600 K. Vertical β -Ga₂O₃ Schottky barrier diodes (SBDs) were fabricated with a bevel-field-plated edge termination, where a beveled sidewall was implemented in both the mesa and the field plate oxide. The Schottky barrier height was found to increase from 1.2 eV to 1.3 eV as the temperature increases from 300 K to 600 K, indicating the existence of barrier height inhomogeneity. The net donor concentration in the drift region shows little dependence on the temperature. The reverse leakage current up to 500 V was found to be limited by both the thermionic-field electron injection at the Schottky contact and the electron hopping via the defect states in the depletion region. At 300–500 K, the leakage is first limited by the electron injection at low voltages and then by the hopping in depleted Ga₂O₃ at high voltages. At temperatures above 500 K, the thermionic field emission limits the device leakage over the entire voltage range up to 500 V. Compared to the state-of-the-art SiC and GaN SBDs when blocking a similar voltage, our vertical Ga₂O₃ SBDs are capable of operating at significantly higher temperatures and show a smaller leakage current increase with temperature. This shows the great potential of Ga₂O₃ SBDs for high-temperature and high-voltage power applications.

Published by AIP Publishing. <https://doi.org/10.1063/1.5132818>

Ultra-wide-bandgap semiconductor gallium oxide (Ga₂O₃) has emerged as a promising material for next-generation power electronics, due to its high critical electrical field (E_C), controllable doping, and the availability of large-diameter wafers.^{1–3} Recently, an E_C over 5 MV/cm (Ref. 4) and an electron mobility of 176 cm²/Vs (Ref. 5) have been experimentally demonstrated in Ga₂O₃, making Ga₂O₃ particularly attractive for medium- and high-voltage (>600 V) power devices.² A breakdown voltage (BV) over 600 V has been demonstrated in a variety of Ga₂O₃ power devices, including lateral MOSFETs,^{6–9} lateral Schottky barrier diodes (SBDs),¹⁰ vertical power FinFETs,¹¹ and vertical SBDs.^{12–16}

While the room-temperature performance of Ga₂O₃ power devices, i.e., the trade-off between the on-resistance (R_{on}) and BV, is still inferior to that of the state-of-the-art SiC and GaN devices,^{7,12} Ga₂O₃ devices have shown great promise for high-temperature applications. With an ultrawide bandgap of 4.8 eV, the intrinsic carrier density in

Ga₂O₃ is significantly lower than that in Si, SiC, and GaN, allowing Ga₂O₃ to maintain effective doping up to very high temperatures. Before the availability of single-crystalline Ga₂O₃ wafers, polycrystalline Ga₂O₃ has long been used for making high-temperature gas sensors with an operating temperature up to 1000 °C.¹ In addition, thermally stable Schottky barrier contacts have been recently demonstrated for Ga₂O₃ devices with an operating temperature up to 500 °C.¹⁷

However, the majority of previous high-temperature studies on Ga₂O₃ devices have only focused on their forward characteristics. For example, high-temperature forward operations have been demonstrated in lateral Ga₂O₃ MOSFETs^{18,19} and vertical Ga₂O₃ SBDs^{15,17,20,21} up to 300 °C (Ref. 18) and 500 °C,¹⁷ respectively, whereas very few high-temperature demonstrations have been reported on the high-voltage blocking capability of Ga₂O₃ power devices. Higashiwaki *et al.* and Konishi *et al.* demonstrated the blocking characteristics of vertical Ga₂O₃ power diodes up to 200 V at 200 °C,^{15,20} which is the highest blocking

voltage that has been reported in Ga₂O₃ devices for high-temperature operation. This blocking voltage is much lower than the requirement for medium- and high-voltage power applications, indicating that the high-temperature blocking capability of Ga₂O₃ power devices has become a key roadblock for their applications in harsh-environment power systems (e.g., oil drilling, aerospace, etc.). From the viewpoint of device design, this issue could be attributed to the lack of a robust edge termination for Ga₂O₃ power devices, as the crowded electric field (E-field) at the device periphery often leads to a fast leakage increase at high voltages and high temperatures. On the other hand, very little is known about the high-temperature, high-voltage leakage mechanisms in Ga₂O₃ power devices.

In this work, we demonstrate a bevel-field-plated vertical Ga₂O₃ Schottky barrier diode (SBD) operational up to 600 K in both forward conduction and reverse high-voltage (>500 V). Two competing leakage mechanisms were unveiled, one being limited by Schottky barrier contact and dominating the low-voltage leakage behaviors while the other is limited by the depletion region and dominates the high-voltage leakage behaviors. The relation between these two mechanisms at different temperatures has also been systematically analyzed.

The schematic of the vertical Ga₂O₃ SBD fabricated in this work is shown in Figs. 1(a) and 1(b). Compared to the previously demonstrated bevel-field-plated Ga₂O₃ SBDs with only beveled mesas,²² our device also has a beveled sidewall at the field oxide in the vicinity of the Schottky contact, which could spread the crowded E-field at the contact edge.¹² The epitaxial structure consists of a 11-μm thick Si-doped n-Ga₂O₃ layer grown by halide vapor phase epitaxy on a 2-in. Sn-doped n⁺-Ga₂O₃ (001) substrate. The net donor concentration ($N_D - N_A$) in the n-Ga₂O₃ drift region was revealed to be $\sim 1.5 \times 10^{16} \text{ cm}^{-3}$ based on C-V measurements. The device fabrication

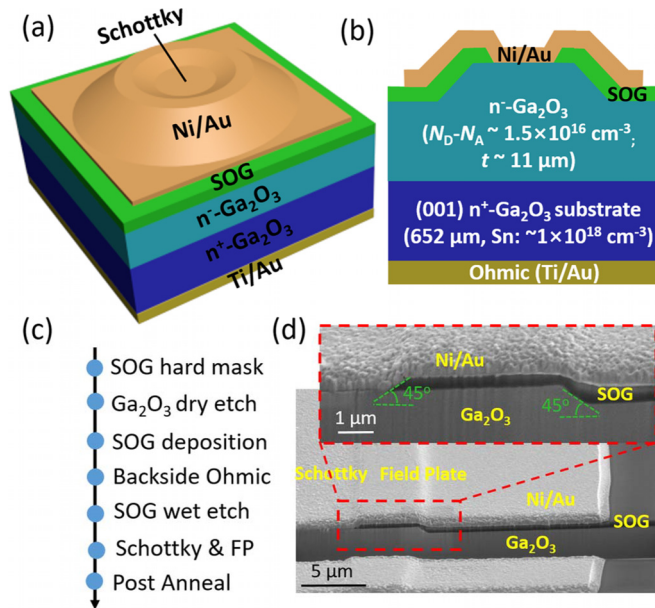


FIG. 1. (a) 3D and (b) cross-sectional schematics of the vertical Ga₂O₃ power SBDs with bevel field plates and mesas. (c) Illustration of the main steps for device fabrication. (d) Cross-sectional scanning electron microscopy image of the device periphery area and the bevel FP and mesa regions.

process is shown in Fig. 1(c). The spin-on-glass (SOG) was first deposited, followed by a patterned wet etch in 4% diluted HF to form the hard mask for mesa etching. The isotropic wet etch forms a $\sim 45^\circ$ angle at the SOG sidewall. $\sim 1 \mu\text{m}$ Ga₂O₃ mesa etch was then performed in an Inductively Coupled Plasma—Reactive Ion Etching (ICP-RIE) system using BCl₃ gas. Next, 650-nm thick SOG was deposited again as the field plate (FP) oxide. A blanket backside Ohmic contact was formed by a Ti/Au (30/150 nm) deposition followed by a 470 °C annealing in N₂. The SOG was opened through wet etch and the Ni/Au stack was deposited for the Schottky and the FP metals. Finally, annealing at 350 °C in N₂ was performed. As shown in Fig. 1(d), the fabricated device shows a $\sim 45^\circ$ beveled angle in both the Ga₂O₃ mesa and the SOG FPs. The circular anode diameter is 200–250 μm.

Figure 2(a) shows the forward current-voltage (*I-V*) characteristics of the fabricated Ga₂O₃ SBDs at the temperature (*T*) from 300 K

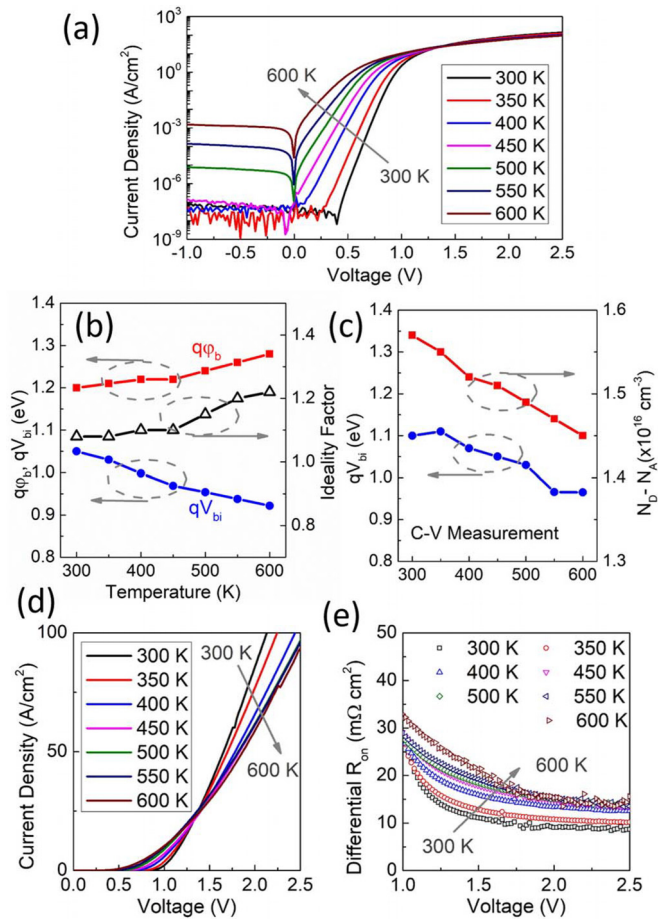


FIG. 2. (a) Forward *I-V* characteristics of the fabricated vertical Ga₂O₃ SBDs at *T* of 300–600 K in a semilog plot. (b) Dependence of the Schottky barrier height, built-in potential, and ideality factor as a function of *T* extracted from the forward *I-V-T* characteristics. (c) Dependence of the built-in potential and the net donor concentration in the drift region as a function of *T* extracted from C-V-T characteristics. (d) Forward *I-V-T* characteristics in a linear plot. (e) The extracted differential R_{on} at *T* of 300–600 K.

to 600 K. The forward I - V - T characteristics can be well fitted by the thermionic emission (TE) model,^{15,20,21}

$$J = J_s \exp\left(\frac{q(V - JR_s)}{nkT}\right) = A^* T^2 \exp\left(-\frac{q\phi_b}{kT}\right) \exp\left(\frac{q(V - JR_s)}{nkT}\right), \quad (1)$$

where J , J_s , k , R_s , and A^* are the current density, saturation current density, Boltzmann constant, series resistance, and effective Richardson constant, respectively. A^* is used as $41 \text{ A}/(\text{cm}^2 \text{ K}^2)$ for Ga_2O_3 in this work.^{20,21} The Schottky barrier height ($q\phi_b$) and ideality factor (n) can be obtained by fitting the $\ln(J)$ vs V in the linear range of the semilog plot.²¹ With the extracted $q\phi_b$, the built-in potential (V_{bi}) is given by²⁰

$$qV_{bi} = q\phi_b - (E_C - E_f) = q\phi_b - kT \ln\left(\frac{N_C}{N_D - N_A}\right), \quad (2)$$

where N_C is the effective density of states in the conduction band of Ga_2O_3 , which can be calculated as a function of T .²⁰ Figure 2(b) shows the extracted $q\phi_b$, V_{bi} , and n of the fabricated vertical Ga_2O_3 SBDs at different T . $q\phi_b$ increases from $\sim 1.2 \text{ eV}$ at 300 K to $\sim 1.3 \text{ eV}$ at 600 K. n increases from 1.08 to 1.21 from 300 K to 600 K. This phenomenon can be attributed to the Schottky barrier height inhomogeneity that has been commonly observed in Ga_2O_3 ^{21,23} and GaN ²⁴ SBDs. At low T , electrons preferentially flow through the lower barriers. As T increases, electrons gain sufficient thermal energy to overcome the higher barriers, leading to a higher $q\phi_b$ extracted from I - V characteristics.

Capacitance-voltage (C - V) measurements were performed from 300 K to 600 K. Based on the linear extrapolation of the $1/C^2$ - V data, V_{bi} and $N_D - N_A$ can be extracted.²⁰ Figure 2(c) shows the extracted V_{bi} and $N_D - N_A$ at 300–600 K. V_{bi} shows a similar value compared to that extracted from the I - V characteristics. It decreases with the increasing T , agreeing with other reports in the literature.²⁰ The changes in $N_D - N_A$ in the drift region are very minimal as a function of T , indicating that most of the donors and acceptors have been fully ionized in the room temperature.

Figure 2(d) shows the forward I - V - T characteristics plotted in the linear scale, and Fig. 2(e) shows the extracted differential specific R_{on} . The R_{on} increases from $\sim 8.5 \text{ m}\Omega\text{-cm}^2$ to $\sim 13.5 \text{ m}\Omega\text{-cm}^2$ as T increases from 300 K to 600 K, mainly due to the mobility degradation at higher T . At $T > 400 \text{ K}$, the R_{on} increases slowly with T , indicating the existence of a compensation mechanism that counters the impact of mobility degradation. From the backside circular transmission-line measurements, the Ohmic contact resistance was found to show little dependence on T . This indicates that the compensation is probably due to the increased donor ionization at high T . As $N_D - N_A$ in the drift region does not increase with T , the increased donor ionization is likely to occur in the n^+ - Ga_2O_3 substrate. This could also explain the minimal increase^{23,25} or even reduction^{26,27} in the R_{on} of vertical Ga_2O_3 SBDs at higher T reported by other groups. The recently observed deep-level 110 meV unintentional donor in the Ga_2O_3 substrate possibly accounts for this increased ionization at high T .²⁸

Figure 3(a) shows the typical reverse I - V characteristics of the fabricated vertical Ga_2O_3 SBDs at room temperature. The leakage current is limited by the source of electrons injected from the metal into Ga_2O_3 and the electron transport in the depleted space region. The schematic illustration of these leakage mechanisms is shown in

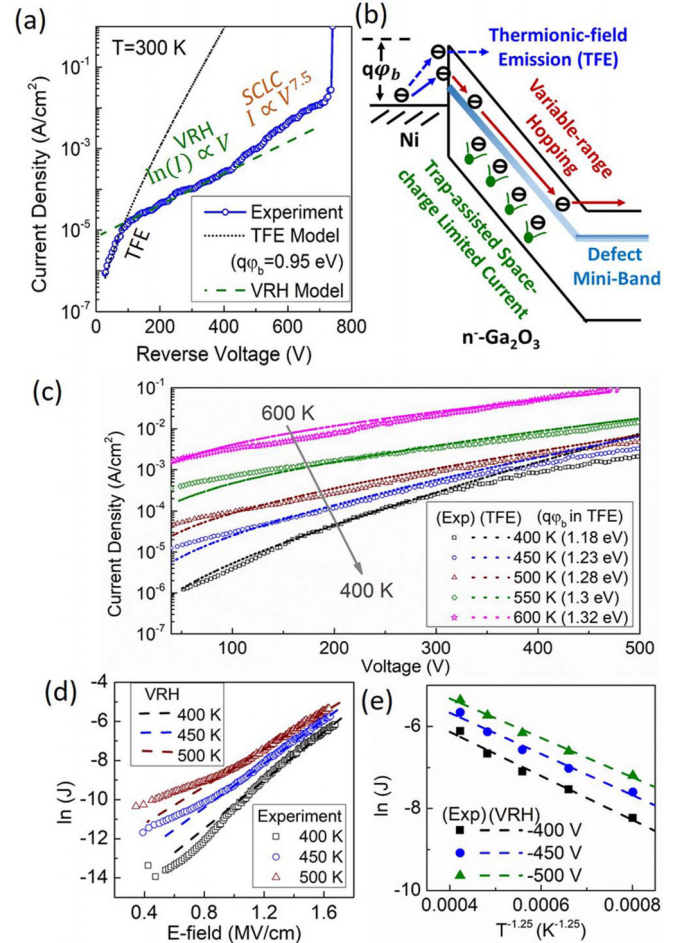


FIG. 3. (a) Typical reverse I - V characteristics of the fabricated vertical Ga_2O_3 SBDs at room temperature and the fitting based on the TFE and variable-range-hopping (VRH) model. (b) Schematic illustration of TFE, VRH, and trap-assisted space-charge-limited conduction (SCLC) mechanisms. The solid blue line represents the TFE and VRH being in series. The dashed blue line represents the TFE to conduction band at 550 K and 600 K. (c) Reverse I - V - T characteristics at 400–600 K up to 500 V and the fitting based on the TFE model. (b) Reverse current density (J) vs the peak E-field at the Schottky contact in a semilog plot at 400, 450, and 500 K. (c) $\ln(J)$ vs $T^{-1.25}$ for the J extracted at the reverse biases of 400, 450, and 500 V.

Fig. 3(b). At low reverse bias ($< 100 \text{ V}$), the leakage current is limited by the source of electrons, as it can be well fitted by the thermionic field emission (TFE) model, which takes into account the barrier lowering and the E-field induced tunneling at the Schottky contact,²⁰

$$J_{TFE} = \frac{A^* T q h E}{2k\pi} \sqrt{\frac{\pi}{2m^* kT}} \times \exp\left(-\frac{q}{kT} \left(\phi_b - \Delta\phi_{bl,0} - \frac{q(hE)^2}{24m^*(2\pi kT)^2}\right)\right), \quad (3)$$

where h and m^* are Planck's constant and the electron effective mass in Ga_2O_3 , respectively. E and $\Delta\phi_{bl,0}$ are the E-field at the Schottky

contact at the reverse bias V and the barrier lowering at zero reverse bias, respectively, which are given by²⁰

$$E = \sqrt{2q(N_D - N_A)(V_{bi} - V)/\epsilon_s}, \quad (4)$$

$$\Delta\phi_{bl,0} = \sqrt[4]{(N_D - N_A)V_{bi}/8q\pi^2\epsilon_s^3}, \quad (5)$$

where ϵ_s is the electric permittivity of Ga_2O_3 . The $N_D - N_A$ and V_{bi} extracted from C - V measurements are used here.

At the reverse bias above 100 V, the leakage current exhibits a $\ln(I) \propto V$ relation. This indicates that the leakage current starts to be limited by the electron transport in the depletion region and the dominant leakage mechanism to be the electron variable-range-hopping (VRH) through defect-related states (dislocation or traps).^{29,30} This mechanism can be depicted by electron hopping via a localized “defect mini-band,”²⁹ as shown in Fig. 3(b). A similar VRH through threading dislocations has been identified to be a major leakage mechanism in vertical GaN power SBDs³¹ and PN diodes.^{29,32} It is worth mentioning that, at lower reverse bias (<100 V), the $q\phi_b$ in the TFE model that provides the best fit to experimental data, 0.95 eV, is lower than the Schottky barrier height extracted from forward I - V characteristics (~ 1.2 eV). This indicates that most of the electrons were injected into the defect mini-band rather than the conduction band.

When the reverse bias is above ~ 500 V, the leakage current becomes higher than the VRH fitting. With an accumulated amount of electrons trapped in the depletion region, the current gradually becomes limited by space charge conduction. This trap-assisted space-charge-limited conduction (SCLC) mechanism is supported by a $I \propto V^n$ relation.³³ This leakage mechanism has also been observed in vertical GaN power SBDs,³⁴ PN diodes,^{35,36} and FinFETs.³⁷ The device ultimate breakdown is destructive and occurs at the device edge, which is limited by the peak E-field in the FP oxide.¹²

To study the high-temperature leakage mechanisms of our Ga_2O_3 SBDs, I - V measurements were performed up to a reverse bias of 500 V up to 600 K. Figure 3(c) shows the experimental reverse I - V - T characteristics from 400 K to 600 K and the fitted curves based on the TFE model. At 400 K and 450 K, the leakage current shows TFE-like behaviors at the reverse biases below 300 V, indicating that it is limited by the source of electrons, and then deviates toward the bulk semiconductor limited mechanism at high biases. The fitted energy barrier is getting closer to the Schottky barrier height at higher T , indicating an increased injection into the conduction band compared to the injection into the defect mini-band. When T increases further (550 K and 600 K), the TFE model agrees with the device leakage over the entire voltage range and the fitted energy barrier is almost identical to the Schottky barrier height extracted from forward I - V - T characteristics. This indicates that the leakage is dominated by the TFE to conduction band.

To verify if VRH dominates the high-voltage leakage at 300–500 K, we investigated the dependence of the leakage current on both the E-field and T . The field- and T -dependence of the VRH current is described by^{29,38}

$$J_{VRH} = J_0 \exp \left[C \frac{eEa}{2kT} \left(\frac{T_0}{T} \right)^{1/4} \right], \quad (6)$$

where J_0 is the low-field current density, T_0 is a characteristic temperature parameter, C is a constant, and a is the localization radius of the

electron wave function. Figure 3(d) plots the $\ln(I)$ vs the peak E-field in the depletion region calculated by (4), which shows a good linear dependence when the peak E-field is above 1 MV/cm (corresponding to the reverse voltage over ~ 300 V). Figure 3(e) plots the $\ln(I)$ vs $T^{-1.25}$ at the reverse biases of 400–500 V, which shows good linear dependence. These results validate the VRH mechanism at high reverse voltages at 300–500 K.

To further understand the impacts of biases and temperatures on the leakage limitation by either the source of electrons or their bulk transport, we look at the VRH drift velocity (v_d), which can be modeled using a Gaussian disorder model,^{29,39}

$$v_d = \mu E \approx \frac{v_0 b}{2} \exp \left(-\frac{\sigma^2}{(kT)^2} \right) \left[\exp \left(\frac{qbE}{kT} \right) - 1 \right], \quad (7)$$

where v_0 is the hopping frequency, b is the average trap-to-trap distance, σ is the energy sigma, and E is the electric field. From (7), a higher temperature will lead to an increased v_d at the same E-field (bias) and therefore, a smaller transit time in the depletion region. This suggests that the leakage current can be less limited by the bulk transport at the same voltage. As a result, the characteristic voltage, at which the TFE-like electron-source limited current transitions into the VRH-like bulk-limited current, increases with temperature. This agrees well with the experiment, as this characteristic voltage increases from ~ 100 V at 300 K to ~ 270 V at 400 K. At even higher T , the transient time is even smaller, and electrons are less localized at the defect mini-band. As a result, the TFE to conduction band dominates the leakage.

Figure 4 compares the maximum operational temperature vs the maximum reverse bias reported for the Ga_2O_3 ,^{15,20,27,40} GaN,^{31,41} and SiC^{42,43} based Schottky barrier power rectifiers. Our work presents the best combination of high-voltage and high-temperature performance in Ga_2O_3 power diodes and our highest operating temperature exceeds the ones reported for GaN and SiC SBDs with a similar operation voltage. When T increases from 300 K to 500 K, the leakage current of our Ga_2O_3 SBDs only increases by about tenfold at 500 V, while at least 100-fold leakage increase at 500 V is shown in vertical GaN^{31,41} and SiC⁴² SBDs with a similar BV. It is also worth mentioning that the

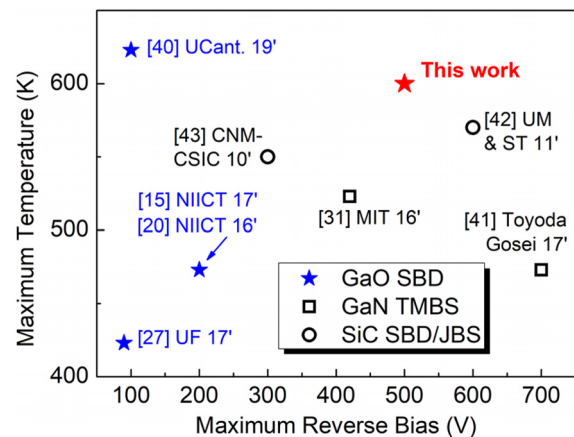


FIG. 4. The maximum operational temperature vs the maximum reverse bias reported for Ga_2O_3 , GaN, and SiC based Schottky barrier power rectifiers.

high-temperature GaN and SiC SBDs typically have more complicated device designs, such as trench metal-oxide-semiconductor barrier Schottky (TMBS) or junction barrier Schottky (JBS) structures, while our Ga₂O₃ SBDs use a much simpler edge termination. These comparisons show the great potential of Ga₂O₃ SBDs for high-temperature and high-voltage power applications.

In summary, this work presents the high-temperature forward and reverse characteristics of the high-voltage vertical Ga₂O₃ SBDs with the bevel-field-plate edge termination. $q\phi_b$ increases with T at 300–600 K, indicating the existence of barrier height inhomogeneity. The leakage current was found to be limited by both the electron injection at the Schottky contact and the electron transport in the depletion region. At 300–500 K, the TFE at the Schottky contact dominates the leakage current at low voltages and the VRH in the depletion region dominates the leakage current at high voltages. At 500–600 K, the TFE model fits the leakage current over the entire voltage range up to 500 V. The high-voltage leakage current in our Ga₂O₃ SBDs shows a smaller increase with T when compared to the state-of-the-art GaN and SiC SBDs, showing the great potential of Ga₂O₃ power rectifiers for high-temperature power applications.

This work was supported by the Southeastern Center for Electrical Engineering Education program and the High Density Integration industry mini-consortium of the Center for Power Electronics Systems at Virginia Tech.

REFERENCES

- ¹S. J. Pearton, J. Yang, P. H. Cary, F. Ren, J. Kim, M. J. Tadjer, and M. A. Mastro, *Appl. Phys. Rev.* **5**, 011301 (2018).
- ²S. J. Pearton, F. Ren, M. Tadjer, and J. Kim, *J. Appl. Phys.* **124**, 220901 (2018).
- ³M. Higashiwaki and G. H. Jessen, *Appl. Phys. Lett.* **112**, 060401 (2018).
- ⁴X. Yan, I. S. Esqueda, J. Ma, J. Tice, and H. Wang, *Appl. Phys. Lett.* **112**, 032101 (2018).
- ⁵Y. Zhang, F. Alema, A. Mauze, O. S. Koksaldi, R. Miller, A. Osinsky, and J. S. Speck, *APL Mater.* **7**, 022506 (2019).
- ⁶K. Zeng, A. Vaidya, and U. Singiseti, *IEEE Electron Device Lett.* **39**, 1385 (2018).
- ⁷K. Tetzner, E. Bahat Treidel, O. Hilt, A. Popp, S. Bin Anooz, G. Wagner, A. Thies, K. Ickert, H. Gargouri, and J. Wurfl, *IEEE Electron Device Lett.* **40**, 1503 (2019).
- ⁸M. H. Wong, K. Sasaki, A. Kuramata, S. Yamakoshi, and M. Higashiwaki, *IEEE Electron Device Lett.* **37**, 212 (2016).
- ⁹N. Moser, J. McCandless, A. Crespo, K. Leedy, A. Green, A. Neal, S. Mou, E. Ahmadi, J. Speck, K. Chabak, N. Peixoto, and G. Jessen, *IEEE Electron Device Lett.* **38**, 775 (2017).
- ¹⁰Z. Hu, H. Zhou, Q. Feng, J. Zhang, C. Zhang, K. Dang, Y. Cai, Z. Feng, Y. Gao, X. Kang, and Y. Hao, *IEEE Electron Device Lett.* **39**, 1564 (2018).
- ¹¹Z. Hu, K. Nomoto, W. Li, N. Tanen, K. Sasaki, A. Kuramata, T. Nakamura, D. Jena, and H. G. Xing, *IEEE Electron Device Lett.* **39**, 869 (2018).
- ¹²N. Allen, M. Xiao, X. Yan, K. Sasaki, M. J. Tadjer, J. Ma, R. Zhang, H. Wang, and Y. Zhang, *IEEE Electron Device Lett.* **40**, 1399 (2019).
- ¹³W. Li, Z. Hu, K. Nomoto, R. Jinno, Z. Zhang, T. Q. Tu, K. Sasaki, A. Kuramata, D. Jena, and H. G. Xing, in *2018 IEEE International Electron Devices Meeting (IEDM)* (IEEE, 2018), pp. 8.5.1–8.5.4.
- ¹⁴J. Yang, F. Ren, M. Tadjer, S. J. Pearton, and A. Kuramata, *ECS J. Solid State Sci. Technol.* **7**, Q92 (2018).
- ¹⁵K. Konishi, K. Goto, H. Murakami, Y. Kumagai, A. Kuramata, S. Yamakoshi, and M. Higashiwaki, *Appl. Phys. Lett.* **110**, 103506 (2017).
- ¹⁶J. Yang, F. Ren, M. Tadjer, S. J. Pearton, and A. Kuramata, *AIP Adv.* **8**, 055026 (2018).
- ¹⁷C. Fares, F. Ren, and S. J. Pearton, *ECS J. Solid State Sci. Technol.* **8**, Q3007 (2019).
- ¹⁸D. Lei, K. Han, Y. Wu, Z. Liu, and X. Gong, *Appl. Phys. Express* **12**, 041001 (2019).
- ¹⁹M. H. Wong, Y. Morikawa, K. Sasaki, A. Kuramata, S. Yamakoshi, and M. Higashiwaki, *Appl. Phys. Lett.* **109**, 193503 (2016).
- ²⁰M. Higashiwaki, K. Konishi, K. Sasaki, K. Goto, K. Nomura, Q. T. Thieu, R. Togashi, H. Murakami, Y. Kumagai, B. Monemar, A. Koukitu, A. Kuramata, and S. Yamakoshi, *Appl. Phys. Lett.* **108**, 133503 (2016).
- ²¹A. Jayawardena, A. C. Ahyi, and S. Dhar, *Semicond. Sci. Technol.* **31**, 115002 (2016).
- ²²C. Joishi, S. Rafique, Z. Xia, L. Han, S. Krishnamoorthy, Y. Zhang, S. Lodha, H. Zhao, and S. Rajan, *Appl. Phys. Express* **11**, 031101 (2018).
- ²³G. Jian, Q. He, W. Mu, B. Fu, H. Dong, Y. Qin, Y. Zhang, H. Xue, S. Long, Z. Jia, H. Lv, Q. Liu, X. Tao, and M. Liu, *AIP Adv.* **8**, 015316 (2018).
- ²⁴W. Lim, J.-H. Jeong, J.-H. Lee, S.-B. Hur, J.-K. Ryu, K.-S. Kim, T.-H. Kim, S. Y. Song, J.-I. Yang, and S. J. Pearton, *Appl. Phys. Lett.* **97**, 242103 (2010).
- ²⁵Q. He, W. Mu, H. Dong, S. Long, Z. Jia, H. Lv, Q. Liu, M. Tang, X. Tao, and M. Liu, *Appl. Phys. Lett.* **110**, 093503 (2017).
- ²⁶S. Oh, G. Yang, and J. Kim, *ECS J. Solid State Sci. Technol.* **6**, Q3022 (2017).
- ²⁷S. Ahn, F. Ren, L. Yuan, S. J. Pearton, and A. Kuramata, *ECS J. Solid State Sci. Technol.* **6**, P68 (2017).
- ²⁸A. T. Neal, S. Mou, R. Lopez, J. V. Li, D. B. Thomson, K. D. Chabak, and G. H. Jessen, *Sci. Rep.* **7**, 13218 (2017).
- ²⁹Y. Zhang, H. Y. Wong, M. Sun, S. Joglekar, L. Yu, N. A. Braga, R. V. Mickevicius, and T. Palacios, in *2015 IEEE International Electron Devices Meeting (IEDM)* (IEEE, 2015), pp. 35.1.1–35.1.4.
- ³⁰V. Moroz, H. Y. Wong, M. Choi, N. Braga, R. V. Mickevicius, Y. Zhang, and T. Palacios, “The impact of defects in GaN device behavior: Modeling dislocations, traps, and pits,” *ECS J. Solid State Sci. Technol.* **5**(4), P3142 (2016).
- ³¹Y. Zhang, M. Sun, Z. Liu, D. Piedra, M. Pan, X. Gao, Y. Lin, A. Zubair, L. Yu, and T. Palacios, in *2016 IEEE International Electron Devices Meeting (IEDM)* (IEEE, 2016), pp. 10.2.1–10.2.4.
- ³²Y. Zhang, A. Dadgar, and T. Palacios, *J. Phys. Appl. Phys.* **51**, 273001 (2018).
- ³³A. Rose, *Phys. Rev.* **97**, 1538 (1955).
- ³⁴X. M. Shen, D. G. Zhao, Z. S. Liu, Z. F. Hu, H. Yang, and J. W. Liang, *Solid-State Electron.* **49**, 847 (2005).
- ³⁵Y. Zhang, M. Sun, D. Piedra, M. Azize, X. Zhang, T. Fujishima, and T. Palacios, *IEEE Electron Device Lett.* **35**, 618 (2014).
- ³⁶Y. Zhang, M. Yuan, N. Chowdhury, K. Cheng, and T. Palacios, *IEEE Electron Device Lett.* **39**, 715 (2018).
- ³⁷M. Xiao, X. Gao, T. Palacios, and Y. Zhang, *Appl. Phys. Lett.* **114**, 163503 (2019).
- ³⁸D. V. Kuksenkov, H. Temkin, A. Osinsky, R. Gaska, and M. A. Khan, *J. Appl. Phys.* **83**, 2142 (1998).
- ³⁹H. Cordes, S. D. Baranovskii, K. Kohary, P. Thomas, S. Yamasaki, F. Hensel, and J.-H. Wendorff, *Phys. Rev. B* **63**, 094201 (2001).
- ⁴⁰C. Hou, R. A. Makin, K. R. York, S. M. Durbin, J. I. Scott, R. M. Gazoni, R. J. Reeves, and M. W. Allen, *Appl. Phys. Lett.* **114**, 233503 (2019).
- ⁴¹K. Hasegawa, G. Nishio, K. Yasunishi, N. Tanaka, N. Murakami, and T. Oka, *Appl. Phys. Express* **10**, 121002 (2017).
- ⁴²A. Testa, S. De Caro, S. Russo, D. Patti, and L. Torrisi, *Microelectron. Reliab.* **51**, 1778 (2011).
- ⁴³P. Godinon, X. Jorda, M. Vellvehi, X. Perpina, V. Banu, D. Lopez, J. Barbero, P. Brosselard, and S. Masseti, *IEEE Trans. Indust. Electron.* **58**(7), 2582 (2011).